RSC Advances

PAPER

View Article Online
View Journal | View Issue

Check for updates

Cite this: *RSC Adv.*, 2019, **9**, 35751

Promoted dispersion and uniformity of active species on Fe–Ce–Al catalysts for efficient NO abatement†

Xiaobo Wang, *[ab] Caojian Jiang,[a] Jia Wang,[c] Keting Gui[d] and Hywel R. Thomas[b]

Fe–Ce–Al catalysts were synthesized by the co-precipitation method (labeled as Fe–Ce–Al–P), co-impregnation method (Fe–Ce–Al–I), and direct mixing method (Fe–Ce–Al–M), respectively, and used for effective removal of NO. The synthesized catalysts were characterized by many methods including N_2 physisorption, X-ray diffraction (XRD), X-ray photoelectron spectroscopy (XPS), NH_3-temperature programmed desorption (NH_3-TPD), H_2-temperature programmed reduction (H_2-TPR), high-resolution transmission electron microscopy (HR-TEM), and energy dispersive spectroscopy (EDS) mapping. The results show that the synthesis methods greatly influence the catalytic performance of catalysts. The Fe–Ce–Al–P catalyst prepared by the co-precipitation method yields the highest catalytic performance, while the Fe–Ce–Al–I and Fe–Ce–Al–M catalysts exhibit relatively low catalytic activity. The co-precipitation method can promote the accumulation and dispersion of more surface active species on the catalyst surface, and provide smaller particle size of active species and generate more uniform particle size distribution, while these characteristics can't be obtained by the co-impregnation method and direct mixing method. Moreover, the co-precipitation method could produce the highest surface area and enhanced redox ability and surface acidity of the catalyst, which resulted from the high dispersion and uniform distribution of surface active species. These may be the key factors to the superior catalytic performance of the Fe–Ce–Al–P catalyst.

Received 29th August 2019
Accepted 30th October 2019

DOI: 10.1039/c9ra06875a

rsc.li/rsc-advances

Open Access Article. Published on 04 November 2019. Downloaded on 1/20/2026 7:15:19 PM.
This article is licensed under a Creative Commons Attribution-NonCommercial 3.0 Unported Licence.

1. Introduction

Nitrogen oxides (NO_x), as a typical pollutant from the combustion process, have caused severe problems in the environment and to human health.[1] To date, several methods and technologies have been developed to remove NO_x and selective catalytic reduction (SCR) is proven to be the most effective route for NO abatement.[2] The key issue for SCR technology is the catalyst and the currently used catalysts for this process are V_2O_5/TiO_2 or $V_2O_5–WO_3/TiO_2$.[3] Although the $V_2O_5–WO_3–TiO_2$ (VWTi) catalyst system could yield high SCR catalytic activity, it also possesses inherent drawbacks, such as relatively narrow catalytic activity temperature window, the poisonous effect of VO_x to the ecosystem and higher oxidation activity of SO_2 to SO_3.[4] Due to this fact, many highly active and environmentally friendly catalysts without VO_x have been developed and may be an alternative route to solve these problems mentioned above.

According to this view, some transition-metal containing oxides, including FeO_x, CuO_x, MnO_x, CeO_x, and CrO_x, have been designed for the replacement of the commercial SCR catalysts.[5–9] Among them, the Fe-containing catalysts have attracted special attention due to its better catalytic activity, favorable N_2 selectivity and nontoxicity.[9,10] And especially the bimetallic Fe catalysts, including Fe–Mn,[11,12] Fe–Ce,[9,13] Fe–Cu[14] and Fe_x-$W_{1-x}O_\delta$,[15] exhibited superior catalytic activity for the SCR reaction. For the Fe–Ce catalysts, many researchers have widely studied this system from different levels and angles. Jiang *et al.* doped Ce onto Fe/β by a simple impregnation step and found Fe–Ce/β catalyst showed high catalytic activity and better hydrothermal stability.[9] Ma *et al.* supported Fe–Ce on carbon nanotube by an ethanol impregnation method and ascribed its excellent catalytic performance to the crystal CeO_2 and enriched chemisorbed oxygen of catalyst surface.[16] Zhang *et al.* synthesized Fe–S–Ce catalysts using the one-pot method and found the excellent SCR performance had a close relationship with the abundant chemisorbed oxygen and the enhanced surface acidity and redox property.[17] Previous studies for the Fe–Ce catalysts mainly focused on the Fe–Ce mixed metal oxides prepared by the one-pot method and supported Fe–Ce on H-

[a]School of Environmental Science, Nanjing Xiaozhuang University, Nanjing 211171, Jiangsu, China. E-mail: xb_wang88@126.com
[b]Geoenvironmental Research Centre, School of Engineering, Cardiff University, Cardiff, CF24 3AA, UK
[c]College of Chemical Engineering, Nanjing Forestry University, Nanjing 210037, Jiangsu, China
[d]School of Energy and Environment, Southeast University, Nanjing 210096, Jiangsu, China

† Electronic supplementary information (ESI) available. See DOI: 10.1039/c9ra06875a

Open Access Article. Published on 04 November 2019. Downloaded on 1/20/2026 7:15:19 PM.
This article is licensed under a Creative Commons Attribution-NonCommercial 3.0 Unported Licence.

β zeolite and carbon nanotube, respectively, using the impregnation method. It is well known that the catalytic performance of catalysts greatly depends on the synthesis methods, support, precursors, oxidation state and crystallinity of metal oxides.[18] However, for the Fe–Ce–Al catalysts, the effect of catalysts synthesis methods on the catalytic activity is still lack of study, and the research on promoting the uniformity of particle size distribution and dispersion characteristics of surface active species by different synthesis methods to achieve superior catalytic performance is not systematically reported in the literature so far, especially the research on the mechanism of optimizing the physicochemical properties of catalyst by promoting the uniformity and dispersion of surface active species. Therefore, based on the discussion above, it is of great importance to reveal the intrinsic relationship among the component, the structure and the catalytic performance of catalyst resulted from different synthesis methods in the angle of promoting active species dispersion and uniformity on Fe–Ce–Al catalysts.

In the present work, the Fe–Ce/Al_2O_3 catalysts with the same Fe/Ce molar ratio were synthesized by three different synthetic strategies and used in the NH_3-SCR reaction. The relationship between the physicochemical properties resulted from different synthesis methods and the excellent catalytic activity was explored *via* different characterization techniques, such as BET, XRD, H_2-TPR, NH_3-TPD, XPS, HR-TEM, and EDS mapping.

2. Materials and methods

2.1 Catalysts synthesis

2.1.1 Co-precipitation method. 18.04 g $Fe(NO_3)_3 \cdot 9H_2O$ and 38.78 g $Ce(NO_3)_3 \cdot 6H_2O$ were added into 200 mL deionized water simultaneously and dissolved completely to get the mixed solution with the designed molar ratio of Fe : Ce being 1 : 2. And then, 25 g Al_2O_3 power was added to the solution with magnetic stirring for 10 min at 50 °C. Later, the ammonia solution (wt 25%) was gradually added to with continuous stirring until the pH value reached 9–10. After stirring for 1.5 h, the resulting suspension was first dried at 120 °C for 12 h and then air-calcined at 450 °C for 5 h. And then, the calcined samples were compressed into tablet form and finally crushed and sieved to 30–60 mesh size for use. The sample was denoted as Fe–Ce–Al–P.

2.1.2 Co-impregnation method. The synthesis processes were the same as the co-precipitation method described above without adding the ammonia solution (wt 25%) to the solution. The sample was labeled as Fe–Ce–Al–I.

2.1.3 Direct mixing method. 3.56 g Fe_2O_3, 15.36 g CeO_2, and 25 g Al_2O_3 power were simultaneously added into 200 mL deionized water to get the solution with a molar ratio of Fe : Ce = 1 : 2. And then the solution was stirred for 10 min at 50 °C. The following processes were the same as the co-precipitation method mentioned above without adding the ammonia solution (wt 25%) to the solution. The sample was named as Fe–Ce–Al–M.

2.2 Catalyst characterization

N_2 adsorption–desorption was carried out at −196 °C on a Quantachrome Quadrisorb SI instrument.

X-ray diffraction (XRD) patterns were obtained on an X-ray diffractometer (Smartlab 9, Japan) to study the crystal structure of the sample with CuKα radiation in the 2θ range from 10 to 90°.

X-ray photoelectron spectroscopy (XPS) analysis was performed to investigate the surface elements and chemical states of the samples on Thermo Fisher Scientific XPS (EXCALAB 250Xi) spectroscopy.

NH_3-TPD and H_2-TPR experiments were carried out on a Micromeritics Autochem 2920 II instrument to investigate the acidity and redox property of each studied sample. For the H_2-TPR experiments, about 110 mg sample was used and pretreated in N_2 at 200 °C for 1 h. And the data was recorded from 100 to 760 °C with a heating rate of 10 °C min^{-1}. For the NH_3-TPD experiments, about 200 mg sample was used and pretreated with He at 450 °C for 1 h. And the TPD experiment was conducted from 100 to 800 °C with a heating rate of 10 °C min^{-1}.

HR-TEM images and EDS mappings were obtained using a JOEL JEM-2100 electron microscope operated at 200 kv to investigate the microstructure of the samples and the elements dispersion.

2.3 Catalytic activity measurement

SCR activity measurement was accomplished in a fixed bed reactor using a 5 mL sample (30–60 mesh). The simulated flue gas was composed of NH_3 (500 ppm), NO (500 ppm), 3% O_2 and balance N_2. The reactions were executed with a total gas flow rate of 1.5 L min^{-1}. All the data were measured online by a flue gas analyzer (rbr ECOM–J2KN, Germany) under steady state. The NO_x conversion was calculated *via*:

$$C_{NO} = \frac{[NO]_{inlet} - [NO]_{outlet}}{[NO]_{inlet}} \times 100 \quad (1)$$

3. Results and discussions

3.1 Catalytic performance

The NO conversion of Fe–Ce–Al catalysts prepared by different methods is shown in Fig. 1. It can be seen that the Fe–Ce–Al–M catalyst exhibits the lowest NO conversion, which is less than 45.6% at 120–360 °C. And the SCR catalytic activity of the Fe–Ce–Al–I catalyst is greatly improved compared with that of the Fe–Ce–Al–M catalyst. With the increase of reaction temperature, the NO conversion of Fe–Ce/Al_2O_3–I catalyst gradually increases from 26.2% to 88.8% at 120–330 °C and then decreases to 88% at 360 °C. For the Fe–Ce–Al–P catalyst, it yields the highest SCR activity in the whole temperature range. More than 96% NO conversion can be obtained in 270–360 °C. These three catalysts prepared by different methods have the same chemical compositions but show a significant difference in catalytic activity. The results demonstrate that the preparation methods

 This journal is © The Royal Society of Chemistry 2019

Open Access Article. Published on 04 November 2019. Downloaded on 1/20/2026 7:15:19 PM.
This article is licensed under a Creative Commons Attribution-NonCommercial 3.0 Unported Licence.

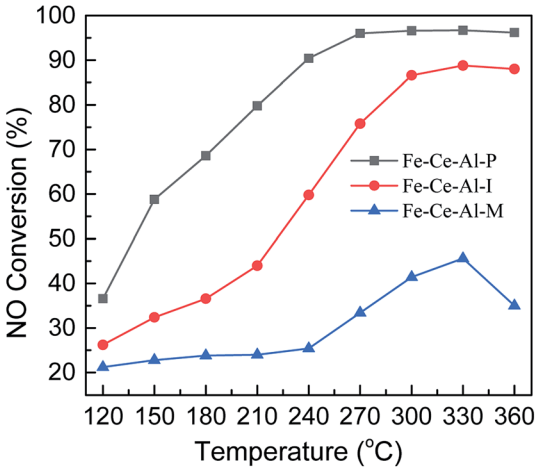

Fig. 1 NO conversion of catalysts prepared by different methods.

have a great effect on its catalytic activity. Furthermore, as shown in Fig. S1,† after a 6 h long reaction at 330 °C, the Fe–Ce–Al–P catalyst still exhibits the best catalytic activity, suggesting the superior activity of the Fe–Ce–Al–P catalyst. The effect of different physicochemical properties of catalysts resulted from the preparation methods on the catalytic performance will be systematically investigated using various characterization technique in the following sections.

3.2 Catalyst characterization

3.2.1 BET surface area and pore size measurements. Table 1 displays the BET surface area, pore volume and pore diameter of the studied samples. Obviously, the Al_2O_3 support exhibits the largest BET surface area (168.30 $m^2\ g^{-1}$) and pore volume (0.27 $mm^3\ g^{-1}$). After the addition of Fe and Ce, the BET surface areas and pore volumes of the studied three samples are decreased due to the dispersion of active species and the sequence is ranked by Fe–Ce–Al–P > Fe–Ce–Al–I > Fe–Ce–Al–M, which is highly consistent with the catalytic performance of catalysts. It indicates that the dispersion of Fe and Ce species on the three catalysts prepared by different methods is different. The larger surface area could provide more surface active sites to promote the adsorption capacity. And big pore volumes could favor the spread of the reaction intermediates and reactant gas.[19] All of these will make the reaction process more efficient and lead to excellent catalytic performance.

Table 1 BET surface area and pore structure results of different samples

Catalysts	S_{BET} ($m^2\ g^{-1}$)	Pore volume ($mm^3\ g^{-1}$)	Pore diameter (nm)
Fe–Ce–Al–P	122.30	0.23	3.72
Fe–Ce–Al–I	94.88	0.20	3.51
Fe–Ce–Al–M	94.09	0.17	3.94
Al_2O_3	168.30	0.27	3.51

3.2.2 X-ray powder diffraction (XRD) analysis. The structural characteristic of different catalysts was investigated by XRD and the results are shown in Fig. 2. For all the Fe–Ce–Al catalysts, no visible characteristic peaks of Fe species can be observed, indicating the iron species are highly dispersed on the surface of catalysts or exist as amorphous. While several strong characteristic peaks attributed to the CeO_2 phase are detected on the catalysts and the same phenomenon can be seen in the XRD patterns of the catalysts after the SCR reaction displayed in Fig. S2.† Compared with those of the Fe–Ce–Al–M catalyst, the peak intensities of the crystal CeO_2 phase are significantly reduced and the peak shapes are broadened on the Fe–Ce–Al–I and Fe–Ce–Al–P catalysts, suggesting that the crystallinity of catalyst is reduced and the coalescence of particles is inhibited.[19,20] The results discussed above clearly indicate that the preparation method has a significant effect on the crystal structure of catalysts. Moreover, the particle size of the catalyst is calculated with the Scherrer equation and the corresponding results are listed in Table 2. It turns out that the crystallite size of the main crystal CeO_2 phase is calculated to be 6.8, 7.4, and 59.6 nm for the Fe–Ce–Al–P, Fe–Ce–Al–I, and Fe–Ce–Al–M catalyst, respectively. And compared with that of Fe–Ce–Al–M catalyst, the full-width-half-maximum (FWHM) of crystal CeO_2 peak over the Fe–Ce–Al–P and Fe–Ce–Al–I catalysts is greatly broadened. It demonstrates that there is a strong interaction between Ce and Fe and this effect inhibits the growth of the crystalline CeO_2 phases on one hand; and on the other hand, compared with direct mixing method, the co-precipitation method and co-impregnation method could lead to different degrees of local distortion and result in different physical properties of CeO_2 such as the crystallite size.[9,19,21] Fe–Ce–Al–P catalyst generates the smallest particle size and would lead to better dispersion of active species. And the results of this effect are that the specific surface area of the catalyst is enlarged and therefore the catalytic performance is enhanced.

3.2.3 X-ray photoelectron spectroscopy (XPS) analysis. XPS analysis was used to explore the valence states and chemical

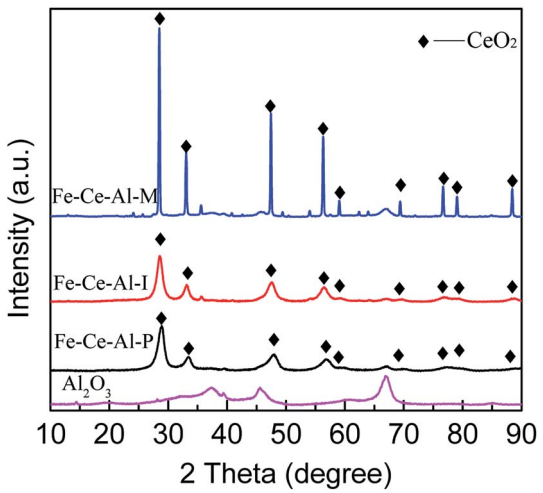

Fig. 2 XRD patterns of different Fe–Ce–Al catalysts and Al_2O_3 support.

Open Access Article. Published on 04 November 2019. Downloaded on 1/20/2026 7:15:19 PM.
This article is licensed under a Creative Commons Attribution-NonCommercial 3.0 Unported Licence.

Table 2 Crystalline sizes of different catalysts

Catalysts	2 Theta (°)	Area	FMWH (rad)	*D* (nm)
Fe–Ce–Al–P	28.68	181 128	1.22	6.8
Fe–Ce–Al–I	28.56	173 729	1.11	7.4
Fe–Ce–Al–M	28.47	269 135	0.17	59.6

Table 3 XPS results of the Fe–Ce–Al catalysts

	Binding energy (eV)			Surface atomic ratio (%)		
	Fe 2p		O 1s			
Catalysts	Fe^{3+}	Fe^{2+}	O_α	$Fe^{3+}/(Fe^{3+}+Fe^{2+})$	$Ce^{3+}/(Ce^{3+}+Ce^{4+})$	$O_\alpha/(O_\alpha+O_\beta)$
Fe–Ce–Al–P	711.5	710.5	531.8	68.62	37.91	42.72
Fe–Ce–Al–I	712.5	710.7	531.8	38.47	19.16	27.99
Fe–Ce–Al–M	713.5	710.8	532.6	18.24	17.29	20.28

components of the samples and the results are displayed in Fig. 3 and Table 3.

The Fe 2p spectra for the investigated catalysts are shown in Fig. 3(a). Two characteristic peaks located at about 710.8–711.3 eV and 723.8–725 eV could be ascribed to Fe $2p_{3/2}$ and Fe $2p_{1/2}$, respectively. And the spectra of Fe $2p_{3/2}$ can be fitted into two sub-bands. The peak locates at about 710.5 eV is attributed to Fe^{2+}, while the peak at about 712.5 eV is ascribed to the Fe^{3+}, indicating the coexistence of FeO and Fe_2O_3 on the surface of studied samples.[22] Moreover, compared with that of the Fe–Ce–Al–I and Fe–Ce–Al–M catalysts, the binding energies for Fe^{2+} and Fe^{3+} over Fe–Ce–Al–P catalyst are shifted to lower values, indicating the Fe species on the surface of Fe–Ce–Al–P catalyst prepared by co-precipitation method are more active, which will help to promote the catalytic performance.[7] The relative proportions of Fe^{3+} and Fe^{2+} were calculated by the peak area of Fe $2p_{3/2}$ for Fe^{3+} and Fe^{2+} (listed in Table 3). The $Fe^{3+}/(Fe^{3+}+Fe^{2+})$ over the Fe–Ce–Al–P catalyst is 68.62%, while it is only 38.47% and 18.24% for the Fe–Ce–Al–I and Fe–Ce–Al–M catalysts, respectively. It indicates that the Fe–Ce–Al–P catalyst prepared by the co-precipitation method can generate more Fe^{3+} species on the catalyst surface. And more Fe^{3+} sites could promote the conversion of NO to NO_2 during the SCR reaction and thus enhance the catalytic activity through the "Fast SCR" reaction.[22,23]

The XPS spectra of the Ce 3d for the three catalysts are displayed in Fig. 3(b), which all can be fitted into peaks labeled as u, u_1, u_2, u_3, v, v_1, v_2, and v_3, respectively. The peaks denoted as

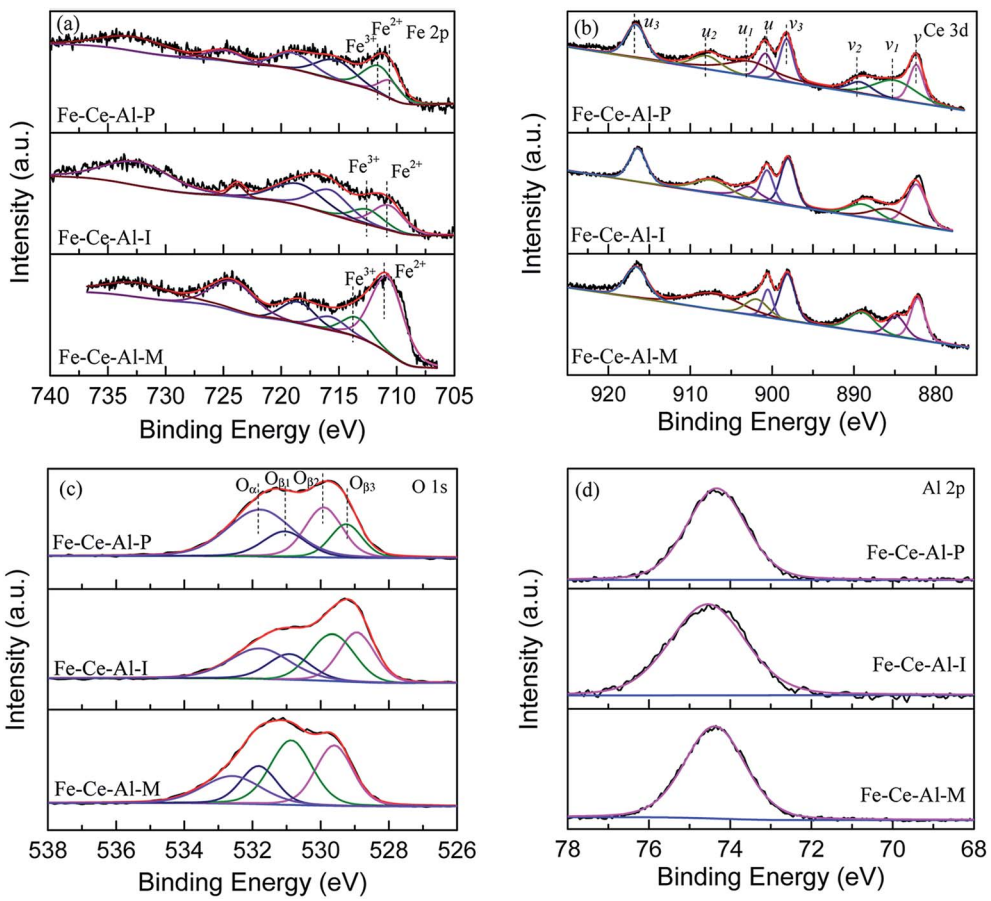

Fig. 3 XPS spectra of (a) Fe 2p, (b) Ce 3d, (c) O 1s and (d) Al 2p for Fe–Ce–Al catalysts.

This journal is © The Royal Society of Chemistry 2019

Open Access Article. Published on 04 November 2019. Downloaded on 1/20/2026 7:15:19 PM.
This article is licensed under a Creative Commons Attribution-NonCommercial 3.0 Unported Licence.

u_1 and v_1 are attributed to the Ce^{3+}, while others are ascribed to Ce^{4+}, suggesting the coexistence of the Ce^{4+} and Ce^{3+} on the catalyst surface. In addition, the $Ce^{3+}/(Ce^{4+} + Ce^{3+})$ ratio over the three samples is decreased as follows: Fe–Ce–Al–P (37.91%) > Fe–Ce–Al–I (19.16%) > Fe–Ce–Al–M (17.29%). It fully indicates that the contents of Ce^{3+} species are closely related to the preparation methods of the catalysts and more Ce^{3+} species can be generated on the catalyst surface by the co-precipitation method. On one hand, more Ce^{3+} species can generate more charge imbalance and oxygen vacancies on the catalyst surface, leading to the enhancement of surface chemisorbed oxygen and therefore facilitation of NO oxidation;[21,24,25] on the other hand, more surface Ce^{3+} species can promote the adsorption of NO and NH_3, and thus contribute to the enhancement of catalytic activity.[26,27] These may be the reasons for the superior catalytic activity of the Fe–Ce–Al–P catalyst.

The O 1s spectra of the studied samples after peak fitting is shown in Fig. 3(c) can be separated into two groups. The peak O_α located at about 532 eV is assigned to the surface adsorbed oxygen, such as O_2^{2-}, OH, and O^- species;[1,28] while the peak O_β centered at about 530 eV is ascribed to the lattice oxygen.[29] After further peak fitting, the peak O_β can be divided into three peaks labeled as $O_{\beta1}$, $O_{\beta2}$ and $O_{\beta3}$, respectively. The $O_{\beta1}$ recorded at about 529.3 ± 0.3 eV is originated from the CeO_2,[30–32] and the $O_{\beta2}$ located at 529.9 ± 0.3 eV can be attributed to oxygen species corresponding to the Fe_2O_3;[33–36] while the $O_{\beta3}$ at about 531 eV can be assigned to the Al–O bonds of Al_2O_3.[37–42] Additionally, the sequence of the relative amount of O_α is ranked by Fe–Ce–Al–P > Fe–Ce–Al–I > Fe–Ce–Al–M catalyst. As the most active catalyst, the Fe–Ce–Al–P catalyst is provided with the highest content of surface adsorbed oxygen with the lowest binding energy, implying the improved oxygen mobility, which is beneficial to promote SCR performance.

The XPS spectra of Al 2p for different samples are detailed in Fig. 3(d). The binding energies of the Al 2p are all centered at about 74.4 ± 0.1 eV. The basically unchanged binding energies of Al 2p demonstrates that the synergistic effect between Fe and Ce species is dominant over the catalysts.

Based on the XPS discussion above, the Fe–Ce–Al–P catalyst possesses the highest content of Fe^{3+} and Ce^{3+}, the redox couples between Fe^{3+}/Fe^{2+} and Ce^{4+}/Ce^{3+} may enhance the redox cycle, which would accelerate the electron transfer and promote the generation of oxygen vacancy, and therefore facilitate the catalytic performance.[29,43]

3.2.4 NH_3-TPD analysis. The surface acidity of catalysts was determined by the NH_3-TPD experiment and the corresponding results are exhibited in Fig. 4. All the NH_3-TPD curves of catalysts after peak fitting contain six NH_3 desorption peaks within the temperature of 100–800 °C, which are related to weak acids (<300 °C), medium acids (300–500 °C), and strong acids (>500 °C), respectively.[4,22,44] For comparison, the total amount of acidity of catalysts is calculated and the total acidity of Fe–Ce–Al–P, Fe–Ce–Al–I, and Fe–Ce–Al–M catalysts is 0.431, 0.386, and 0.354 mmol g^{-1}, respectively. Despite having the same components, the surface acidity obviously differs on each catalyst with different preparation methods, suggesting the co-precipitation treatment could enhance the total amount of acidity,

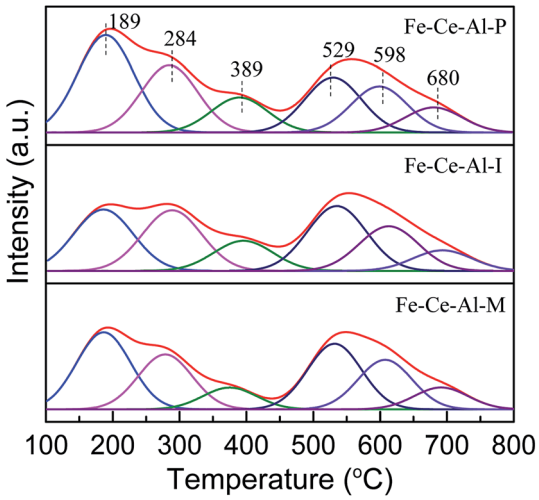

Fig. 4 NH_3-TPD profiles of different catalysts.

especially the weak and moderate acidity (depicted in Table 4). As expected, the SCR activity is highly consistent with the order of the total amount of acidity. Based on the BET, XRD, and XPS results, the co-precipitation method can promote the dispersion of active species and generate small particle size, and thus result in a large surface area. Therefore, the Fe–Ce–Al–P catalyst could provide more acid sites and promote the adsorption of NH_3 on the catalyst surface, thereby could exhibit superior catalytic activity.

3.2.5 H_2-TPR analysis. The redox properties of catalysts were evaluated by H_2-TPR analysis and the results are depicted in Fig. 5. It can be clearly seen that all H_2-TPR profiles of the catalysts exhibit five reduction peaks after peaking fitting in the whole temperature range. For the Fe–Ce–Al–P catalyst, the reduction peaks at 236 and 312 °C are assigned to the reduction process of chemisorbed oxygen and $Fe_2O_3 \rightarrow Fe_3O_4$.[16] And the peaks featured at 446 °C is associated with the reduction of the surface CeO_2.[2,16] While the reduction peaks at high temperatures (556 and 621 °C) are assigned to the reduction of $Fe_3O_4 \rightarrow$ FeO and the FeO → Fe overlap with those originating from the reduction of bulk CeO_2, respectively.[2,16] For the profiles of the Fe–Ce–Al–I catalyst, the reduction behavior is similar to that of the Fe–Ce–Al–P catalyst but the corresponding reduction peaks of Fe and Ce species shift towards higher temperatures. And this reduction characteristics are more pronounced on the Fe–Ce–Al–M catalyst in the low temperature (<500 °C). For comparison, the total consumption of H_2 was calculated and

Table 4 Quantitative data of the NH_3-TPD profiles of catalysts

	Acidity (mmol g^{-1})			
Catalysts	Weak	Moderate	Strong	Total
Fe–Ce–Al–P	0.218	0.046	0.167	0.431
Fe–Ce–Al–I	0.167	0.041	0.178	0.386
Fe–Ce–Al–M	0.161	0.026	0.167	0.354

Open Access Article. Published on 04 November 2019. Downloaded on 1/20/2026 7:15:19 PM.
This article is licensed under a Creative Commons Attribution-NonCommercial 3.0 Unported Licence.

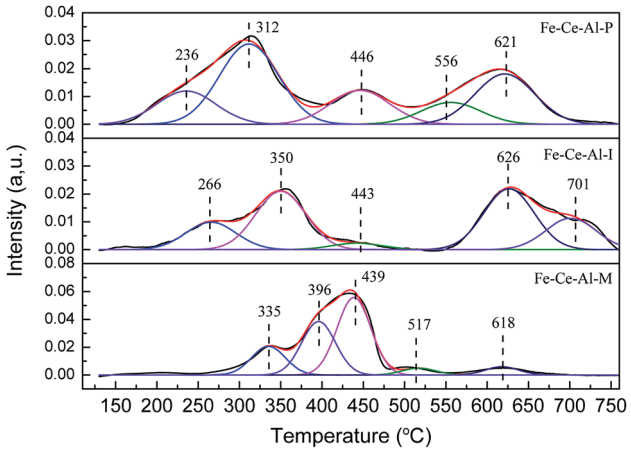

Fig. 5 H_2-TPR profiles of different catalysts.

the data are as follows: Fe–Ce–Al–P (0.69 mmol g^{-1}) > Fe–Ce–Al–I (0.43 mmol g^{-1}) > Fe–Ce–Al–M (0.42 mmol g^{-1}). These results indicate that the Fe–Ce–Al–P catalyst yields the best redox ability, while that of the Fe–Ce–Al–I and Fe–Ce–Al–M catalyst is relatively reduced at low temperature. It is accepted that a change for the reduction peak position can be affected by many factors, such as particle sizes, structural defects, the content of surface oxygen and phase component.[45] Based on the XPS and XRD results, it may be due to the fact that the Fe–Ce–Al–P catalyst has smaller particle sizes and better dispersion of active species, and higher surface oxygen content. Therefore the catalyst can exhibit enhanced redox ability and yield superior catalytic performance.

3.2.6 HR-TEM analysis. The micrographs and size distribution of different samples were obtained by HR-TEM analysis and the results of different scales and particle size distribution are shown in Fig. 6 and S3.† For the Fe–Ce–Al–P catalyst, it consists of uniform nanoparticles with the average particle size of 7.59 nm and displays well dispersion; and the shape of the particles for Fe–Ce–Al–I catalyst are irregularly containing some long strips particles. The average particle size is calculated to be 12.00 nm and some nanoparticles exist slight surface agglomeration. For the Fe–Ce–Al–M catalyst, the particle size distribution is extremely irregular and some large particles (>200 nm) could be observed, suggesting the poor dispersed nature of Fe and Ce species. Moreover, the resulting HR-TEM images of three catalysts shown in Fig. S4† exhibit the lattice fringes with interplanar distances of 0.31 nm corresponding to (1 1 1) planes of bulk CeO_2.[46] These results are well consistent with the XRD results and demonstrate that the particle size and dispersion of active species are greatly dependent on the catalyst preparation method. The Fe–Ce–Al–P catalyst prepared by the co-precipitation method can generate better dispersion of active species and more uniform size distribution of nanoparticles. In general, the smaller particle size and better dispersion of active species will lead to better catalytic performance. On one hand,

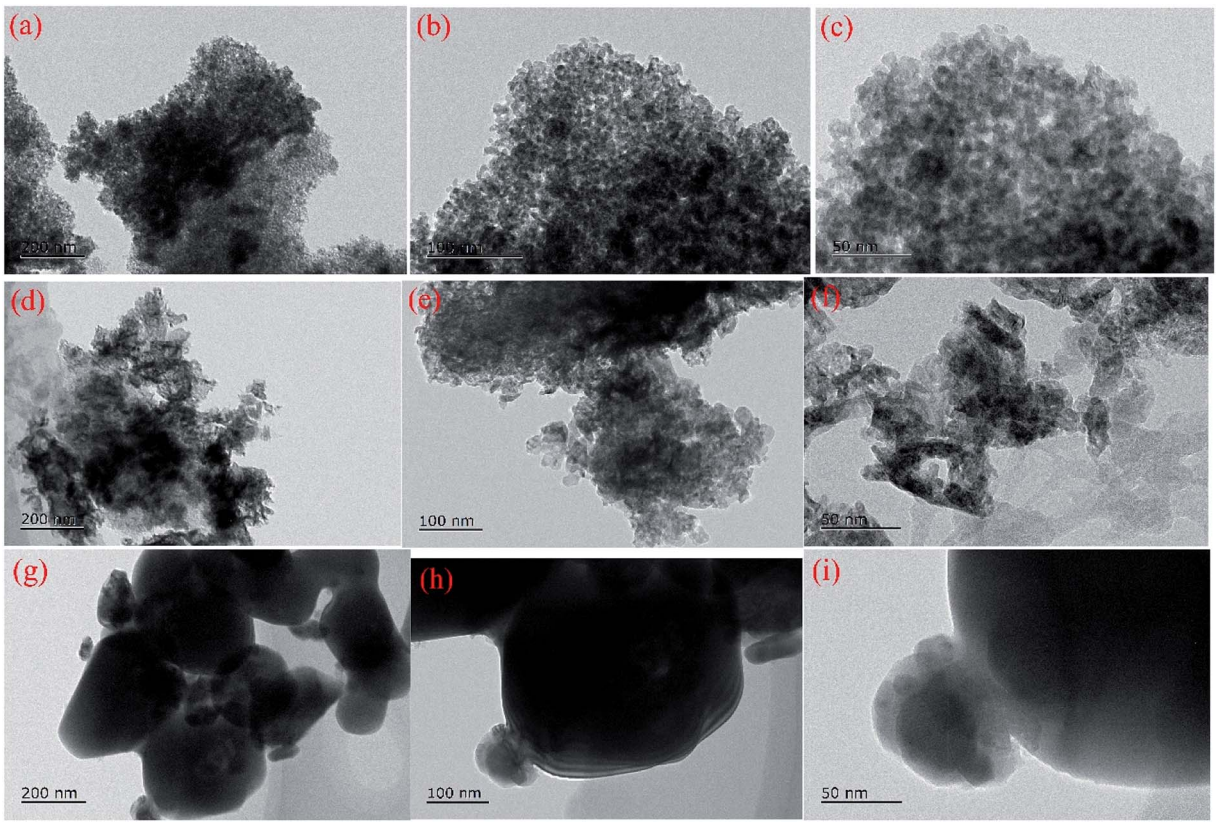

Fig. 6 TEM profiles of different catalysts (a–c) Fe–Ce–Al–P, (d–f) Fe–Ce–Al–I, and (g–i) Fe–Ce–Al-M.

This journal is © The Royal Society of Chemistry 2019

Open Access Article. Published on 04 November 2019. Downloaded on 1/20/2026 7:15:19 PM.
This article is licensed under a Creative Commons Attribution-NonCommercial 3.0 Unported Licence.

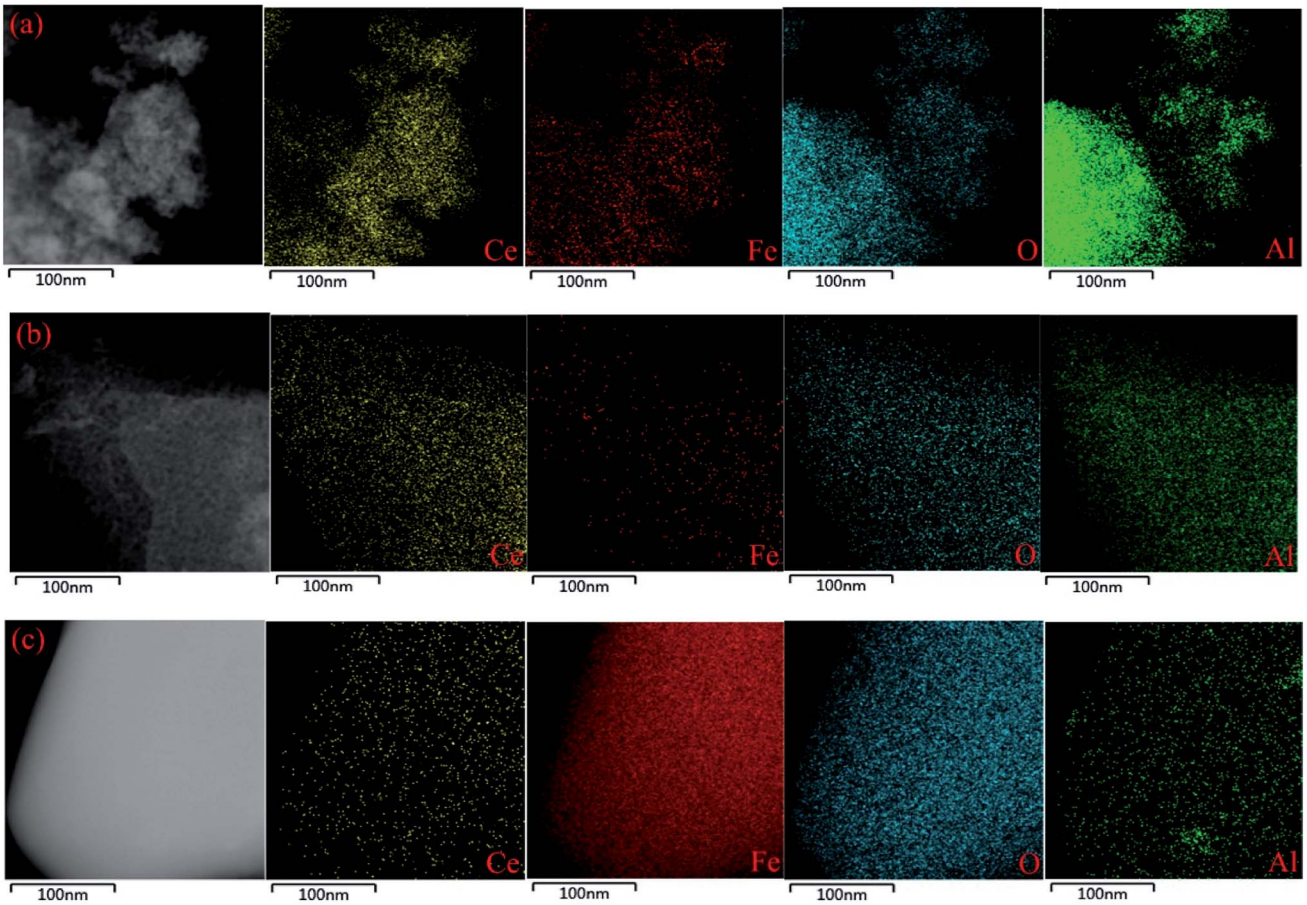

Fig. 7 TEM-EDS mapping results of different catalysts: (a) Fe–Ce–Al–P, (b) Fe–Ce–Al–I, and (c) Fe–Ce–Al–M.

the smaller particle size and better dispersion will generate a bigger surface area and thus provide more active sites. Therefore, more reactant gas molecule can be adsorbed in the catalyst surface and promote the catalytic performance; on the other hand, the redox ability of catalyst plays an important role in the SCR reaction. The redox ability of catalyst can be enhanced by smaller particle size and better dispersion of active species and thus will contribute to the enhanced the catalytic activity of the catalyst. In short, the co-precipitation method could generate smaller particle size and high dispersion of active species and therefore could exhibit superior catalytic performance.

3.2.7 EDS mapping analysis. EDS mapping was carried out to investigate different elements dispersion of catalysts and provide further evidence of different dispersion of active species over Fe–Ce–Al catalysts as depicted in Fig. 7. For the Fe–Ce–Al–P catalyst, the colored dots representing the concentration of Fe, Ce, and O elements, respectively, are dispersed highly and uniformly on the sample surface, while this phenomenon is not present in the Fe–Ce–Al–I and Fe–Ce–Al–M catalysts. Compared with that of the Fe–Ce–Al–P catalyst, the Fe–Ce–Al–I and Fe–Ce–Al–M catalyst exhibit poor dispersion and uniformity of active species. It can be seen from Fig. 7(b) and (c) that less Fe is dispersed on the Fe–Ce–Al–I catalyst surface compared to other elements, while Ce exhibits poor dispersion on the Fe–Ce–Al–M catalyst surface and serious Fe aggregation occurs on its surface. These results demonstrate that the dispersion of active species on the surface of the Fe–Ce–Al–P catalyst is significantly better than that of Fe–Ce–Al–P and Fe–Ce–Al–I catalyst. Moreover, the SEM-EDS mapping results of the catalysts after the SCR reaction shown in Fig. S5† demonstrate that the Fe–Ce–Al–P catalyst still possesses the best dispersion of active species. On the basis of the characterization results of XRD, TEM, and EDS mapping, it can draw the conclusion that the co-precipitation method could inhibit the crystallinity of particles and improve the dispersion of active species compared with the other two methods, and therefore promote the catalytic activity of the catalyst.

4. Conclusion

In this work, Fe–Ce–Al catalysts were prepared by three different methods and the synthesis methods have a direct impact on the catalytic performance of catalysts. The Fe–Ce–Al–P catalyst prepared by the co-precipitation method yields the highest catalytic performance, while the Fe–Ce–Al–I and Fe–Ce–Al–M catalyst exhibit relatively low denitration efficiency. Compared with that of Fe–Ce–Al–I and Fe–Ce–Al–M catalyst, the Fe–Ce–Al–

Open Access Article. Published on 04 November 2019. Downloaded on 1/20/2026 7:15:19 PM.
This article is licensed under a Creative Commons Attribution-NonCommercial 3.0 Unported Licence.

P catalysts before and after the reaction possess the best dispersion of active species and more surface active species are accumulated on the surface of Fe–Ce–Al–P catalyst. And the Fe–Ce–Al–P catalyst could provide smaller particle sizes of active species and generate more uniform particle sizes distribution, all mentioned above may be the key factors to the superior catalytic performance. Moreover, the co-precipitation method could produce the highest surface area and the enhanced redox ability and surface acidity of the catalyst due to the high dispersion and uniform distribution of surface active pieces, and these characteristics will also directly contribute to the superior catalytic performance of Fe–Ce–Al–P catalyst.

Conflicts of interest

There are no conflicts to declare.

Acknowledgements

This work was supported by the National Natural Science Foundation of China (51276039), the Natural Science Foundation of the Jiangsu Higher Education Institutions of China (17KJB610005), the Jiangsu Government Scholarship for Overseas Studies (JS-2018), and a project funded by Nanjing Xiaozhuang University (2016NXY41).

References

1 J. Liu, R. T. Guo, M. Y. Li, P. Sun, S. M. Liu, W. G. Pan, S. W. Liu and X. Sun, *Fuel*, 2018, **223**, 385–393.
2 L. J. France, Q. Yang, W. Li, Z. Chen, J. Guang, D. Guo, L. Wang and X. Li, *Appl. Catal., B*, 2017, **206**, 203–215.
3 R. T. Guo, X. Sun, J. Liu, W. G. Pan, M. Y. Li, S. M. Liu, P. Sun and S. W. Liu, *Appl. Catal., A*, 2018, **558**, 1–8.
4 S. Han, Q. Ye, S. Cheng, T. Kang and H. Dai, *Catal. Sci. Technol.*, 2017, **7**, 703–717.
5 F. Cao, S. Su, J. Xiang, P. Wang, S. Hu, L. Sun and A. Zhang, *Fuel*, 2015, **139**, 232–239.
6 L. Zhu, L. Zhang, H. Qu and Q. Zhong, *J. Mol. Catal. A: Chem.*, 2015, **409**, 207–215.
7 B. Shen, F. Wang and T. Liu, *Powder Technol.*, 2014, **253**, 152–157.
8 R. Yang, H. Huang, Y. Chen, X. Zhang and H. Lu, *Chin. J. Catal.*, 2015, **36**, 1256–1262.
9 S.-Y. Jiang and R.-X. Zhou, *Fuel Process. Technol.*, 2015, **133**, 220–226.
10 B. Feng, Z. Wang, Y. Sun, C. Zhang, S. Tang, X. Li and X. Huang, *Catal. Commun.*, 2016, **80**, 20–23.
11 S. Yang, F. Qi, S. Xiong, H. Dang, Y. Liao, P. K. Wong and J. Li, *Appl. Catal., B*, 2016, **181**, 570–580.
12 W. Mu, J. Zhu, S. Zhang, Y. Guo, L. Su, X. Li and Z. Li, *Catal. Sci. Technol.*, 2016, **6**, 7532–7548.
13 Y. Shu, T. Aikebaier, X. Quan, S. Chen and H. Yu, *Appl. Catal., B*, 2014, **150–151**, 630–635.
14 T. Zhang, J. Liu, D. Wang, Z. Zhao, Y. Wei, K. Cheng, G. Jiang and A. Duan, *Appl. Catal., B*, 2014, **148–149**, 520–531.
15 H. Wang, Z. Qu, S. Dong, H. Xie and C. Tang, *Environ. Sci. Technol.*, 2016, **50**, 13511–13519.
16 Y. Ma, D. Zhang, H. Sun, J. Wu, P. Liang and H. Zhang, *Ind. Eng. Chem. Res.*, 2018, **57**, 3187–3194.
17 X. Zhang, J. Wang, Z. Song, H. Zhao, Y. Xing, M. Zhao, J. Zhao, Z. a. Ma, P. Zhang and N. Tsubaki, *Mol. Catal.*, 2019, **463**, 1–7.
18 S. S. R. Putluru, L. Schill, A. D. Jensen, B. Siret, F. Tabaries and R. Fehrmann, *Appl. Catal., B*, 2015, **165**, 628–635.
19 W. Zhao, Q. Zhong, Y. Pan and R. Zhang, *Chem. Eng. J.*, 2013, **228**, 815–823.
20 S. Andreoli, F. A. Deorsola, C. Galletti and R. Pirone, *Chem. Eng. J.*, 2015, **278**, 174–182.
21 K. Chen, R. Chen, H. Cang, A. Mao, Z. Tang and Q. Xu, *Environ. Technol.*, 2018, **39**, 1753–1764.
22 H. Xu, Y. Li, B. Xu, Y. Cao, X. Feng, M. Sun, M. Gong and Y. Chen, *J. Ind. Eng. Chem.*, 2016, **36**, 334–345.
23 G. Delahay, D. Valade, A. Guzmanvargas and B. Coq, *Appl. Catal., B*, 2005, **55**, 149–155.
24 T. Wang, H. Liu, X. Zhang, Y. Guo, Y. Zhang, Y. Wang and B. Sun, *Fuel Process. Technol.*, 2017, **158**, 199–205.
25 H. Li, C.-Y. Wu, Y. Li and J. Zhang, *Appl. Catal., B*, 2012, **111–112**, 381–388.
26 Z. Song, Q. Zhang, P. Ning, J. Fan, Y. Duan, X. Liu and Z. Huang, *J. Taiwan Inst. Chem. Eng.*, 2016, **65**, 149–161.
27 C. Liu, L. Chen, H. Chang, L. Ma, Y. Peng, H. Arandiyan and J. Li, *Catal. Commun.*, 2013, **40**, 145–148.
28 P. Sun, S. X. Huang, R. T. Guo, M. Y. Li, S. M. Liu, W. G. Pan, Z. G. Fu, S. W. Liu, X. Sun and J. Liu, *Appl. Surf. Sci.*, 2018, **447**, 479–488.
29 T. Wang, Z. Wan, X. Yang, X. Zhang, X. Niu and B. Sun, *Fuel Process. Technol.*, 2018, **169**, 112–121.
30 R. Eloirdi, P. Cakir, F. Huber, A. Seibert, R. Konings and T. Gouder, *Appl. Surf. Sci.*, 2018, **457**, 566–571.
31 G. Praline, B. E. Koel, R. L. Hance, H. I. Lee and J. M. White, *J. Electron Spectrosc. Relat. Phenom.*, 1980, **21**, 17–30.
32 H. L. Dauscher, F. L. Normand, W. Müller, G. Maire, A. Vasquez, *et al.*, *Surf. Interface Anal.*, 1990, **16**, 341–346.
33 W. Liu, M. Zhu, J. Liu, X. Li and J. Liu, *Chin. Chem. Lett.*, 2019, **30**, 750–756.
34 K. Park, H. Y. Hong, G. W. Jung, D. H. Kim, D. A. Hakeem and A. Iqbal, *Ceram. Int.*, 2018, **44**, 15024–15034.
35 H. Liu, Z. G. Zhang, X. X. Wang, G. D. Nie, J. Zhang, S. X. Zhang, N. Cao, S. Y. Yan and Y. Z. Long, *J. Phys. Chem. Solids*, 2018, **121**, 236–246.
36 X. Zhang, Y. Yang, L. Song, Y. Wang, C. He, Z. Wang and L. Cui, *Mol. Catal.*, 2018, **447**, 80–89.
37 H. Y. Yu, M. F. Li, B. J. Cho, C. C. Yeo, M. S. Joo, D. L. Kwong, J. S. Pan, C. H. Ang, J. Z. Zheng and S. Ramanathan, *Appl. Phys. Lett.*, 2002, **81**, 376–378.
38 N. M. Figueiredo, N. J. M. Carvalho and A. Cavaleiro, *Appl. Surf. Sci.*, 2011, **257**, 5793–5798.
39 J. Ding, C. Yu, J. Liu, C. Deng and H. Zhu, *Mater. Chem. Phys.*, 2018, **206**, 193–203.
40 C. K. Gao, J. Y. Yan, L. Dong and D. J. Li, *Appl. Surf. Sci.*, 2013, **285**, 287–292.

 This journal is © The Royal Society of Chemistry 2019

Open Access Article. Published on 04 November 2019. Downloaded on 1/20/2026 7:15:19 PM.
This article is licensed under a Creative Commons Attribution-NonCommercial 3.0 Unported Licence.

41 I. Iatsunskyi, M. Kempiński, M. Jancelewicz, K. Załęski, S. Jurga and V. Smyntyna, *Vacuum*, 2015, **113**, 52–58.
42 X. Zhu, J. Yu, C. Jiang and B. Cheng, *Phys. Chem. Chem. Phys.*, 2017, **19**, 6957–6963.
43 Q. Xu, R. Su, L. Cao, Y. Li, C. Yang, Y. Luo, J. Street, P. Jiao and L. Cai, *RSC Adv.*, 2017, **7**, 48785–48792.
44 K. Zhuang, Y. P. Zhang, T. J. Huang, B. Lu and K. Shen, *J. Fuel Chem. Technol.*, 2017, **45**, 1356–1364.
45 F. Xia, Z. Song, X. Liu, X. Liu, Y. Yang, Q. Zhang and J. Peng, *Res. Chem. Intermed.*, 2018, **44**, 2703–2717.
46 A. Phuruangrat, S. Thongtem and T. Thongtem, *Mater. Lett.*, 2017, **196**, 61–63.